Journal of Solid State Chemistry **147,** 501–508 (1999)
Article ID jssc.1999.8404, available online at http://www.idealibrary.com on IDEAL®

Synchrotron X-Ray Powder Diffraction Study of $(Bi,Pb)_{1.64}Sr_{1.43}Ca_{1.57}Mn_2O_9$, Mn-Analogue of BSCCO-2212 Superconductor

M. Catti,*[,1] D. Levy,† and G. Artioli†

*Dipartimento di Scienza dei Materiali, Universitá di Milano-Bicocca, via Cozzi 53, 20125 Milano, Italy; and †Dipartimento di Scienze della Terra, Università di Milano, via Botticelli 23, 20133 Milano, Italy

Received December 12, 1998; in revised form May 19, 1999; accepted June 1, 1999

The orthorhombic Mn-2212 phase, with nominal composition $BiPbSr_{1.8}CaMn_{2.1}O_9$, was synthesized by solid state reaction. Synchrotron X-ray powder diffraction data ($\lambda = 0.9359$ Å) were collected at Brookhaven National Laboratory (U.S.A.) and used for a structure Rietveld refinement ($a = 5.3314(3)$, $b = 5.3697(2)$, $c = 31.067(2)$ Å). Convergence was obtained in space groups *Fmmm*, *Amaa*, and *Abmm* ($Z = 4$) with the same agreement indexes ($wR_p = 0.0216$, $R_p = 0.0158$, $R(|F|^2) = 0.0419$). The two lower symmetry structure models correspond to different descriptions of partial ordering of oxygen atoms in the (Bi,Pb)–O layer. Refined site occupancies indicate a phase composition close to $(Bi_{1-y}Pb_y)_{1.64}(Sr_{0.33}Ca_{0.67})_2(Sr_{0.77}Ca_{0.23})Mn_2O_9$, with y between 0.4 and 0.5. This result, coupled with electroneutrality requirements, leads to an estimated Mn oxidation state of 3.8 $|e|$. Unlike in Cu-2212, an O atom is present in the (Sr,Ca) plane between adjacent Mn–O layers, producing a distorted octahedral (instead of pyramidal) coordination of Mn.

Key Words: **synchrotron X rays; powder diffraction; Rietveld refinement; superconductors; $BiPbSr_{1.8}CaMn_{2.1}O_9$.**

INTRODUCTION

The study of copper replacement by other first-row transition metals in high-T_c superconductors has attracted a lot of interest since the discovery of such phases, although it soon appeared that the superconductivity is normally destroyed upon complete Cu substitution. The main aim for the investigation of such substituted phases is to understand the relationship among their crystal-chemical properties, the atomic valences, and the nature of the charge-transfer mechanism between the rocksalt blocks and the superconducting layers in the presence of the transition metal substitution. Mn^{3+} is a particularly attractive candidate for Cu^{2+} replacement as (i) it shows a similar Jahn–Teller distortion effect, (ii) it is easily oxidized or reduced, thus providing electronic charge carriers, and (iii) it may also display a complex magnetic behavior.

In the family of BSCCO superconductors, the complete Mn^{3+}/Cu^{2+} replacement was fully characterized for the one-layer 2201 structure (1). The two phases $Bi_2Sr_2MnO_{6+x}$ and $BiPbSr_2MnO_6$ were synthesized and studied thoroughly from the structural, magnetic, and spectroscopic points of view in our laboratory and by other authors (2–6). In particular, X-ray absorption spectroscopy (3) and single-crystal X-ray diffraction (2) indicated that charge compensation for the Mn/Cu exchange in the Pb-free compound is provided both by reduction of the formal Mn^{3+} valence (effective charge of $+2.6$ $|e|$) and by a slight excess of oxygen ($x = 0.3$) in the Bi–O layer. The presence of excess oxygen induces an incommensurate modulation of the crystal structure. On the other hand, the structure of the Pb-containing phase is not modulated and is characterized by positional disorder of oxygen in the Bi–O plane, which has stoichiometric composition as shown by neutron diffraction (5). In the latter compound the Mn^{3+}/Cu^{2+} exchange is thus fully compensated by the coupled Pb^{2+}/Bi^{3+} substitution. This interpretation of the Mn charge distribution in the two Mn-2201 compounds was confirmed by EPR and magnetic susceptibility data (6).

The present investigation reports the synthesis and structural characterization of Mn-2212, the analogue of the two-layer BSCCO-2212 phase with nominal composition $BiPbSr_2CaMn_2O_{8+x}$. Unlike in the one-layer Mn-2201 compound, the Pb^{2+}/Bi^{3+} substitution in the two-layer phase is not sufficient to compensate for the charge unbalance due to the Mn^{3+}/Cu^{2+} exchange. An intermediate behavior between those of the $Bi_2Sr_2MnO_{6+x}$ and $BiPbSr_2MnO_6$ phases is therefore to be expected. On the other hand, different mechanisms of charge compensation might also be observed, because the insertion of an extra layer of Ca atoms between the two neighboring Mn–O planes may provide new empty anion sites suitable for excess-oxygen insertion. Moreover, it is interesting to

[1] To whom correspondence should be addressed.

0022-4596/99 $30.00

compare the crystal-chemical features of this phase with those of the well-known corresponding superconducting cuprate. High-resolution powder diffractometry using high-brilliance synchrotron X rays has been employed in order to tackle such complex structural problems.

During the analysis of the diffraction data, we became aware of a recent study of the related compounds $Bi_{2-x}Pb_xSr_{1.5}Ca_{1.5}Mn_2O_{9-\delta}$ with $x = 1$ and 0.5. (7). For the composition $x = 0.5$ an incommensurate structural modulation was detected by transmission electron microscopy, and the average structure was refined by conventional powder X-ray diffraction (Cu$K\alpha$ radiation) in space group *Abmm*. No modulation was reported for the case $x = 1$ and the structure was not refined. Our results by high-resolution synchrotron powder diffraction will be compared with those of previous work (7) and with the average structure of the Cu-2212 phase (8).

EXPERIMENTAL

Synthesis and Conventional X-Ray Diffractometry

The compound (F.W. = 885.37 for $BiPbSr_2CaMn_2O_9$) was prepared by solid-state reaction, starting from a stoichiometric mixture of commercial analytical-grade $SrCO_3$, $CaCO_3$, Bi_2O_3, and PbO, together with Mn_2O_3 obtained by decomposition of MnO_2 at 750°C in air. The powder sample was heated at 800°C for 15 h in a Pt crucible, pressed in a pellet, and thermally treated three times at 950°C (15–20 h each), with intermediate regrinding and pelleting. All thermal cycles were performed in a horizontal tubular furnace under Ar flux to avoid oxidation of Mn^{3+}. After the first heating cycle the conventional powder X-ray diffractogram showed the sample to be composed mainly of the Mn-2201 phase, with a small quantity of the Mn-2212 compound and other $SrMnO_3$ and $Sr_3Mn_2O_7$ impurities. During the subsequent thermal cycles all the Mn-2201 phase transformed gradually into Mn-2212; however, the strontium manganite impurities did not disappear completely. Several attempts to remove these phases were carried out. Raising the temperature of heat treatments was unsuccessful, probably because of the enhanced evaporation of PbO and BiO. The only improvement was obtained by slightly changing the starting composition in the direction of a small excess of Mn and a deficiency of Sr with respect to ideal stoichiometry. Upon increasing the Mn and decreasing the Sr atoms by 5 and 10%, respectively, the $Sr_3Mn_2O_7$ phase disappeared, whereas $SrMnO_3$ dropped to below 10 wt% (as estimated by Bragg peak intensity) but could not be removed completely, similarly to what was reported in Ref. (7). The powder X-ray diffraction pattern, recorded by a Siemens D500 diffractometer with a diffracted beam monochromator (Cu$K\alpha$ radiation, $\lambda = 1.5406$ Å; t(step) = 4 s, $\Delta(2\theta) = 0.02°$), could be indexed on the basis of an orthorhombic unit-cell similar to that of BSSCO-2212. The least-squares refined values of cell-edges are $a = 5.327(5)$, $b = 5.380(3)$, $c = 31.08(2)$ Å. The systematic absences are consistent with space groups *Amaa* (as in the Cu-2212 structure), *Abmm*, or even *Fmmm*. No reflections indicating an incommensurate modulation are observed. In Table 1, the list of observed and calculated d_{hkl} values with relative intensities in the range 1.19–4.00 Å is given, for the material of nominal composition $BiPbSr_{1.8}CaMn_{2.1}O_{8+x}$. The strongest lines of the $SrMnO_3$ impurity phase are (110) at 2.722, (102) at 3.270, and (202) at 2.092 Å. A chemical analysis was performed on the same compound by an R.A.L. Angular Dispersion Electron Microprobe (5 μm beam dimension, 15 kV accelerating voltage and 15 nA referring current). Eighteen point analyses were performed, yielding an average metal atomic composition $Bi_{0.72}Pb_{0.60}Sr_{2.03}$

TABLE 1
Powder Diffraction Pattern of $BiPbSr_{1.8}CaMn_{2.1}O_9$ in the Range $1.19 < d_{hkl} < 4.00$ Å

h	k	l	d_{hkl} (Å)	I/I_{max} (%)
0	0	8	3.883	12
1	1	1	3.756	4
1	1	3	3.554	32
1	1	5	3.231	46
0	0	10	3.107	19
0	1	9	2.904	2
1	1	7	2.879	100
0	2	0	2.685	43
2	0	0	2.666	38
0	2	2	2.646	2
2	0	2	2.627	3
0	0	12	2.589	11
1	1	9	2.550	7
0	2	6	2.383	3
2	0	6	2.370	2
0	0	14	2.219	8
0	2	10	2.031	13
2	0	10	2.023	13
0	0	16	1.942	6
2	2	0	1.892	5
0	2	12	1.864	7
2	0	12	1.857	3
1	1	15	1.817	20
0	2	14	1.710	13
2	0	14	1.705	4
1	3	3	1.674	3
3	1	3	1.665	5
1	3	5	1.637	4
2	2	0	1.361	3
2	2	16	1.355	5
0	4	0	1.342	6
4	0	0	1.333	4
1	3	15	1.313	4
1	3	17	1.243	4
3	3	7	1.213	5
2	4	0	1.199	4
4	2	0	1.194	3

$Ca_{1.02}Mn_{2.00}$, which corresponds to a weighted average of Mn-2212 and (Sr,Ca)MnO_3. This result clearly indicates that a significant loss of Pb and Bi occurs by evaporation during the thermal treatments.

Synchrotron X-Ray Structure Refinement

The powder diffraction profile was collected on beam-line X7B at the National Synchrotron Light Source (Brookhaven National Laboratory, U.S.A.) using a parallel-beam Debye–Scherrer geometry, the sample loaded in a 0.3 mm diameter capillary, and a flat Image Plate detector. The white X-ray beam has been monochromatized using a Si(111) crystal, and the wavelength ($\lambda = 0.93589(2)$ Å) was calibrated by Rietveld refinement of LaB_6 reference material (NIST SRM 660a, assuming $a = 4.15695(6)$ Å at 25°C). The powder pattern of standard LaB_6 was also used to calibrate the sample–detector distance and the detector tilt angle, following a locally developed procedure. The 2-D diffraction rings were converted into a conventional powder pattern by pixel integration along the central strip of the Debye rings and profile interpolation into 2400 fixed 0.01° wide 2θ steps. The suitable angular range is $11^\circ \leq 2\theta \leq 60^\circ$, corresponding to $0.936 \leq d \leq 4.210$ Å.

The Rietveld refinement and the structure analysis were performed by the software package GSAS (9) considering both phases (Mn-2212 and $SrMnO_3$ impurity) in the profile fitting. The anomalous scattering correction ($\Delta f'$ and $\Delta f''$) has been taken into account because of the proximity of the Pb and Bi L_{III} absorption edges ($E = 13.055$ and $E = 13.419$ ke V, respectively) to the incident beam energy ($E = 13.249$ ke V). The $\Delta f'$ and $\Delta f''$ values used for the refinement are -11.526 and 4.04 for Bi, -10.965 and 9.865 for Pb, -1.500 and 0.745 for Sr, 0.0 and 1.2 for Mn, and 0.0 and 0.52 for Ca, respectively, and they were calculated by the program FPRIME included in the GSAS package (9). Such values were kept fixed during the Rietveld least-squares minimization to avoid correlation with atomic displacement parameters and site occupancy factors. The background exhibits a particularly complex angular dependence due to the capillary diffusion, and it was modeled by a Chebyshev polynomial of first kind with 25 coefficients. The Bragg-peak profile was represented by a multiterm Simpson's rule integration (10) of the pseudo-Voigt function (linear combination of Gaussian and Lorentzian functions) (11) corrected for asymmetry (parameter A). The angular variance (σ^2) of the Gaussian component of the peak is $\sigma^2 = U \tan^2\theta + V \tan\theta + W$, and the Lorentzian variance-square-root (γ) varies as $\gamma = X/\cos\theta + Y \tan\theta$. V and Y were set equal to zero, and the parameters U, W, X, A (phase 1), and X, A (phase 2) were simultaneously refined together with the scale factors of both phases.

The structural refinement was first carried out in space group *Amaa* ($Z = 4$; standard orientation, *Cccm*) using the atomic coordinates of the BSCCO-2212 phase as a start, assuming full site occupancies and default average isotropic atomic displacement factors (Uiso = 0.025 for all atoms). As for the minor $SrMnO_3$ phase (space group $P6_3/mmc$), only the lattice constants were refined, while the structural model was constrained to literature values of the atomic coordinates (12). By careful analysis of the refined isotropic atomic displacement parameters and of the difference Fourier maps calculated for the Mn-2212 phase, the following results were extracted from the preliminary refinement: (i) a residual peak with a height corresponding to an oxygen atom was present in the 4*f* position (0,3/4,1/4); (ii) the Ca (4*e*: 0,1/4,1/4) and Sr (8*l*: 0,*y*,*z*) sites were markedly under- and overpopulated in electrons, respectively; (iii) the Bi site (8*l*: 1/2,*y*,*z*) was slightly overpopulated. The structural model was modified accordingly: the additional O5 atom at 0,3/4,1/4 was inserted; Sr was substituted in place of Ca in the 0,1/4,1/4 site, and the occupancy of the site at 0,*y*,*z* was modeled by 50% Sr and 50% Ca. The isotropic refinement at this stage converged rapidly to $wR_p = 0.0269$, $R(|F|^2) = 0.0574$; however, the atomic displacement factors of O3 and O4 refined to slightly negative values. In the subsequent cycles, the occupancy of the (Bi,Pb) site, and the relative proportions of Sr and Ca in the two sites at 0,1/4,1/4 and 0,*y*,*z* (constrained to full occupancy) were included in the refinement. Further, anisotropic displacement factors were used for all metal atoms. On the basis of evidence of positional disorder from difference Fourier maps, the O4 oxygen position was refined according to a split-atom model, leading to a shift of 0.39 Å from the (100) mirror plane. Anisotropic displacement factors could not be used for O atoms, as they made the refinement diverge. The final profile agreement factors were $wR_p = 0.0216$ and $R_p = 0.0158$, while the Bragg reflection $R(|F|^2)$ value was 0.0419 (417 observations, 75 refined parameters). At convergence the obtained weight

TABLE 2
Occupation Factors and Atomic Fractional Coordinates of $BiPbSr_2CaMn_2O_9$ in Space Group *Amaa*

	Site	o.f.	*x*	*y*	*z*
Mn	8*l*	1	0.5	0.2482(42)	0.18718(21)
(Bi,Pb)	8*l*	0.824(8)	0	0.7509(16)	0.04802(9)
Ca1	8*l*	0.67(2)	0	0.2535(42)	0.13034(17)
Sr1	8*l*	0.33(2)	0	0.2535(42)	0.13034(17)
Sr2	4*e*	0.77(3)	0	0.25	0.25
Ca2	4*e*	0.23(3)	0	0.25	0.25
O1	8*h*	1	0.75	0	0.1934(9)
O2	8*h*	1	0.25	0.5	0.1738(7)
O3	8*l*	1	0.5	0.238(15)	0.1155(4)
O4	16*m*	0.5	0.073(5)	0.3821(35)	0.0497(7)
O5	4*f*	1	0	0.75	0.75

Note. The e.s.d.s are given in parantheses. The refined lattice constants are $a = 5.3314(3)$, $b = 5.3697(2)$, $c = 31.067(2)$ Å.

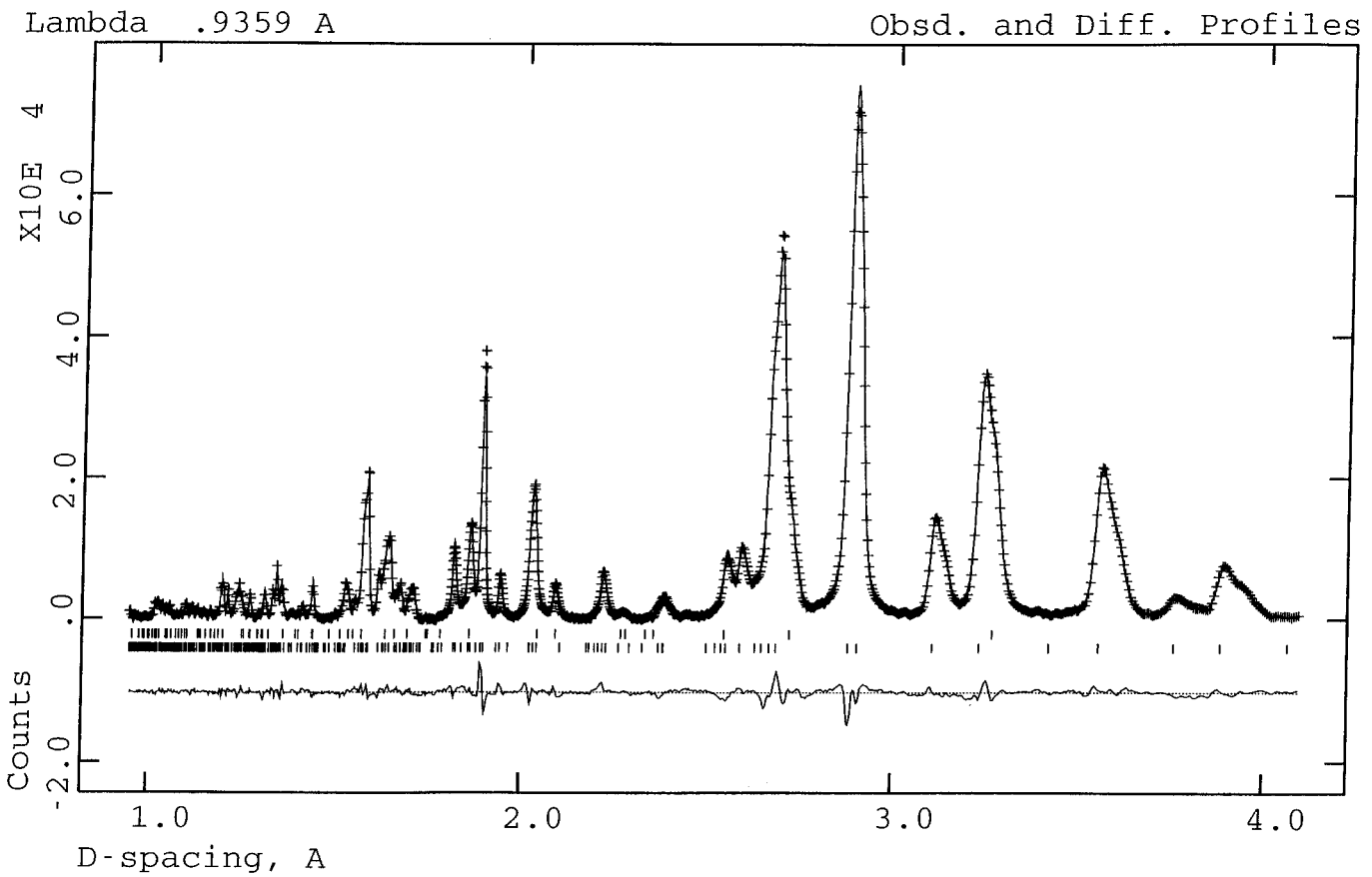

FIG. 1. Observed (crosses), calculated (continuous line), and difference (bottom) powder diffraction profiles of $BiPbSr_{1.8}CaMn_{2.1}O_9$. The positions of Bragg peaks are indicated as vertical marks both for the Mn-2212 phase (lower marks) and for the $SrMnO_3$ impurity (upper marks).

fraction of the $SrMnO_3$ impurity phase was 9.8(1)%. The final refined atomic coordinates and lattice constants are reported in Table 2, and a plot of experimental and calculated powder pattern profiles is shown in Fig. 1. Shoulders are shown by peaks at large d-spacings, which, though enhanced by the d_{hkl} scale on the horizontal axis, could reveal a tendency toward monoclinic splitting of lattice points. This effect might be related to ordering processes in the structure.

A Rietveld refinement was also performed in space group *Abmm* ($Z = 4$; standard orientation *Cmma*), according to the structure model proposed in Ref. (7). According to the symmetry requirements, the O4 oxygen site is split into two disordered positions related by the (010) mirror plane. The results of such refinement are reported in Table 3; the R values obtained at convergence do not differ significantly from those achieved with the refinement in space group *Amaa*. Close inspection of the results in Tables 2 and 3 indicates that atomic shifts from the (010) pseudo-mirror plane at $y = 0.25$ and 0.75 (*Amaa* case), or from the (100) pseudo-mirror plane at $x = 0.25$ and 0.75 (*Abmm* case), are hardly significant except for in the case of the O4 position. This observation led us to consider the disordered structural model in space group *Fmmm*, of which both *Amaa* and *Abmm* are subgroups. This was supported also by recognizing that no extra peaks corresponding to violation of the extinction conditions for *Fmmm* were observed in the synchrotron data. The origin has to be shifted by $-1/2$, $-1/4$, $-1/4$ and by $+1/4$,0, $-1/4$ to pass from *Amaa* and *Abmm*, respectively, to *Fmmm*. Consistent with features of difference Fourier maps, the O4 site is now split twice, according to the scheme shown in Fig. 2, and is thus disordered over four positions related by the (010) and (100) mirror planes. Further, each O1 and O2 is disordered over two positions related by the (001) plane. The *Fmmm* refinement (67 parameters, 266 Bragg peaks) converged to the same R values obtained in the previous cases. The refined structural parameters are reported in Table 4; the displacement factors obtained in the *Amaa* and *Abmm* cases, for the sake of brevity not given in Tables 2 and 3, are quite similar to those shown in Table 4. An absorption correction according to Hewat's empirical formula (13) for the Debye–Scherrer geometry was attempted ($\mu R = 2.0$ for a packing fraction of 1/3 and $R = 0.15$ mm). However, the Rietveld

TABLE 3
Occupation Factors and Atomic Fractional Coordinates of $BiPbSr_2CaMn_2O_9$ in Space Group *Abmm*

	Site	o.f.	*x*	*y*	*z*
Mn	8*m*	1	0.743(6)	0	0.18734(22)
(Bi,Pb)	8*m*	0.826(9)	0.7505(21)	0	0.04800(9)
Ca1	8*m*	0.67(2)	0.7476(44)	0.5	0.13037(17)
Sr1	8*m*	0.33(2)	0.7476(44)	0.5	0.13037(17)
Sr2	4*g*	0.78(3)	0.760(6)	0.5	0.5
Ca2	4*g*	0.22(3)	0.760(6)	0.5	0.5
O1	8*k*	1	0.5	0.25	0.1934(8)
O2	8*j*	1	0	0.25	0.1743(7)
O3	8*m*	1	0.759(20)	0	0.1159(5)
O4	16*o*	0.5	0.829(4)	0.3666(35)	0.0499(7)
O5	4*g*	1	0.740(21)	0	0.25

Note. The e.s.d.s are given in parantheses. Lattice constants are the same as in Table 2.

TABLE 4
Occupation Factors, Atomic Fractional Coordinates, and Anisotropic (Metal Atoms) or Isotropic (Oxygen Atoms) Displacement Factors (10^{-2} Å^2) of $BiPbSr_2CaMn_2O_9$ in Space Group *Fmmm*

	Site	o.f.	*x*	*y*	*z*	U_{11} or U_{iso}	U_{22}	U_{33}
Mn	8*i*	1	0	0	0.06279(21)	4.3(5)	2.3(4)	7.2(4)
(Bi,Pb)	8*i*	0.822(8)	0	0	0.20196(8)	6.4(2)	3.1(2)	3.5(1)
Ca1	8*i*	0.67(2)	0.5	0	0.11970(15)	2.5(5)	0.1(3)	4.0(4)
Sr1	8*i*	0.33(2)	0.5	0	0.11970(15)	2.5(5)	0.1(3)	4.0(4)
Sr2	4*b*	0.77(3)	0.5	0	0	3.4(5)	1.1(3)	6.3(4)
Ca2	4*b*	0.23(3)	0.5	0	0	3.4(5)	1.1(3)	6.3(4)
O1	16*j*	0.5	0.75	0.25	0.0561(8)	2.3(9)		
O2	16*j*	0.5	0.25	0.75	0.0760(7)	0.9(7)		
O3	8*i*	1	0	0	0.1341(5)	4.3(5)		
O4	32*p*	0.25	0.426(4)	0.1353(34)	0.2003(7)	0.1(8)		
O5	4*a*	1	0	0	0	0.5(6)		

Note. The e.s.d.s are given in parantheses. Lattice constants are the same as in Table 2.

refinement converged with great difficulty to $R_p = 0.0232$ and $wR_p = 0.0347$, showing other unsatisfactory features like much larger e.s.d.s, but with no really significant changes for most structural parameters with respect to the values reported in Table 4. For these reasons, the present case was considered to be outside the regime of Hewat's model, and the correction was neglected.

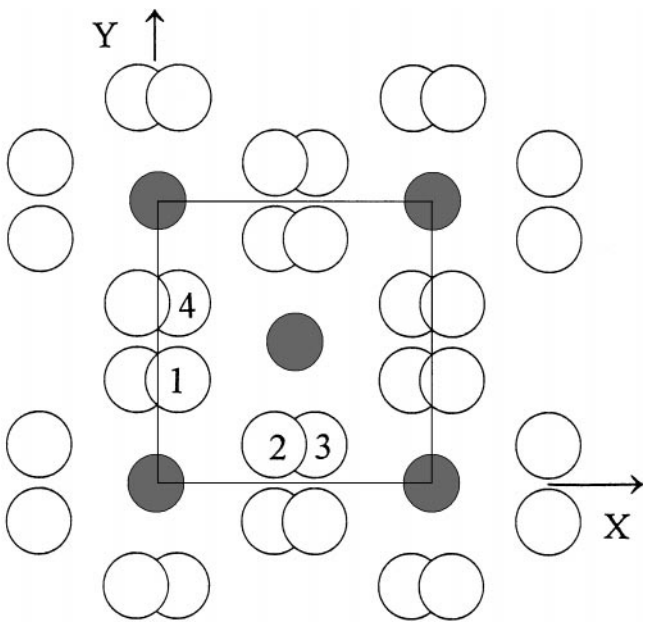

FIG. 2. The structural (Bi,Pb)–O layer, showing the disorder of O4 oxygen atoms (open circles) in the *Fmmm* space group. The numbering corresponds to that given in Table 5.

RESULTS AND DISCUSSION

The crystal structure of $BiPbSr_2CaMn_2O_{8+x}$ could be successfully refined both in the *Fmmm* (double-disorder model) and in the *Amaa* or *Abmm* (single-disorder model) space groups, with rather similar agreement factors. Positional disorder involves primarily the O4 oxygen atom in the (Bi,Pb)–O layers, but also O1 and O2 in the Mn–O layer (*Fmmm* case). The results indicate that different locally ordered configurations of such oxygen atoms are present with comparable probabilities in the average large-scale structure. However, according to our X-ray diffraction data no structural modulation should be coupled to this disorder, in accordance with previous transmission electron microscopy results on similar samples having nominal composition $BiPbSr_{1.5}Ca_{1.5}Mn_2O_{9-\delta}$ (7). The metal atom coordinates of the *Abmm* refinement (Table 3) are in agreement with those of the average structures of the modulated phases $Bi_{1.5}Pb_{0.5}Sr_{1.5}Ca_{1.5}Mn_2O_{9-\delta}$ (7) and $Bi_2Sr_3Fe_2O_9$ (14), while for most oxygen atoms there are substantial differences related mostly to the interpretation of positional disorder. Further, the first of the two phases and its commensurate counterpart $BiPbSr_{1.5}Ca_{1.5}Mn_2O_{9-\delta}$ have lattice constants ($a = 5.359$, $b = 5.344$, $c = 30.976$ Å; $a = 5.408$, $b = 5.322$, $c = 30.979$ Å, respectively) which significantly differ from those of the present compound.

Site Occupancies and Charge Balance

By inspection of Table 2, the crystal structure of the present compound in space group *Amaa* (Fig. 3) appears to be isotypic with that of the Cu-2212 phase (8), with the

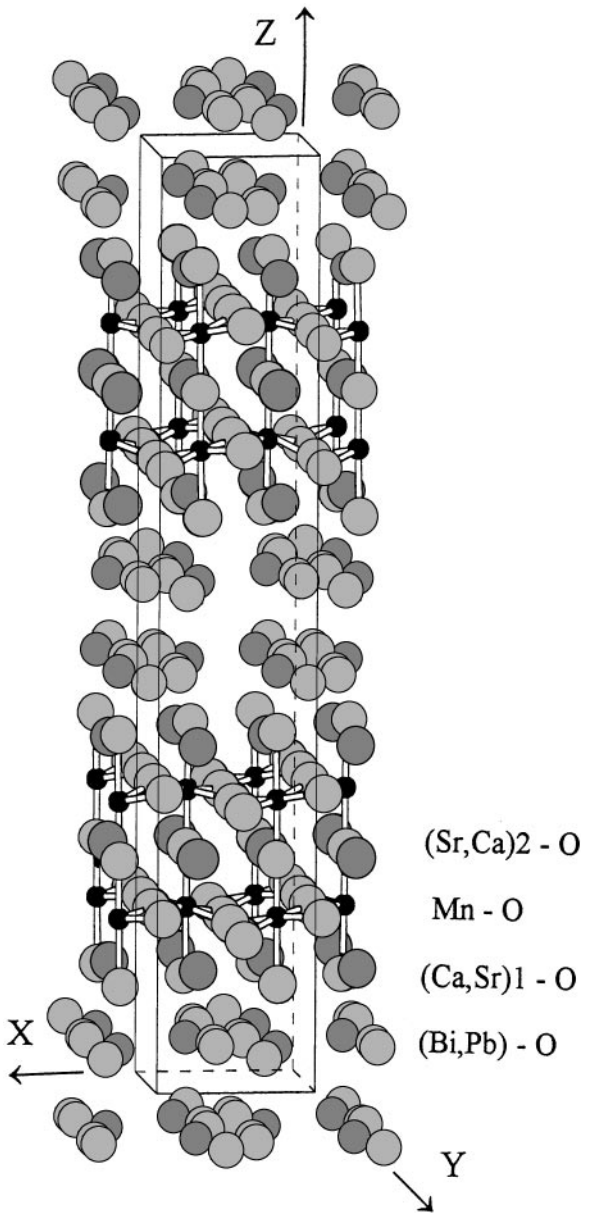

FIG. 3. The crystal structure of $BiPbSr_{1.8}CaMn_{2.1}O_9$ in the *Amaa* representation.

following exceptions. (i) The "Ca layer" at $z = 1/4$, sandwiched between adjacent Mn–O planes, is populated by an additional fully occupied oxygen atom site (O5). This leads to nine oxygen atoms per formula unit. (ii) There is an exchange of Sr and Ca between sites 1 and 2 ("Sr site" and "Ca site" of the Cu-2212 structure, respectively), yielding a proportion of approximately 2/3 Ca: 1/3 Sr on site 1 and 3/4 Sr: 1/4 Ca on site 2. The corresponding chemical composition is $Sr_{1.43}Ca_{1.57}$, and approaches closely that of the previously studied compound (7). (iii) The refined occupancy factor of the (Bi,Pb) site shows a significant deficiency (18%) with respect to ideal stoichiometry. This result is very reliable, taking into account the high scattering power of Bi and Pb atoms, although it is not possible to discriminate their relative proportions on the site because of their close atomic numbers. The loss of these metals is probably due to volatilization during thermal treatments and agrees with results from the microprobe analysis (where the loss is overestimated because it is averaged with the Bi,Pb-free $SrMnO_3$ phase). We tested the possibility of Mn substitution into the (Bi,Pb) site by refining a partial Mn occupancy in that position, but the electron deficiency was not removed and the refinement results worsened significantly.

Results (i) and (ii) are qualitatively similar to those reported for $Bi_{1.5}Pb_{0.5}Sr_{1.5}Ca_{1.5}Mn_2O_{9-\delta}$ (7). On the other hand, the deficiency of metal atoms in the (Bi,Pb)–O layers was not reported in that case, and it affects the overall charge balance of the structure substantially. On the basis of occupancy refinement, we can write the chemical formula of our compound as $(Bi_{1-y}Pb_y)_{1.65}(Sr_{0.33}Ca_{0.67})_2(Sr_{0.77}Ca_{0.23})Mn_2O_9$. The starting nominal content of Bi and Pb (one atom each per formula unit) leads to the constraint $0.394 \le y \le 0.606$, and electroneutrality to $q(\mathrm{Mn}) = 0.825y + 3.525$, by assuming Bi^{3+} and Pb^{2+} oxidation states. It thus turns out that q(Mn) is constrained to lie within the narrow range 3.85 to 4.02 $|e|$. The lower value, corresponding to $y \approx 0.4$, is more probable, as Pb is more volatile than Bi. Thus the manganese valence is expected to be closer to Mn^{4+} than Mn^{3+} in the investigated Mn-2212 phase. This important result is partially due by the loss of heavy metals from the rock salt-type block; in the case of stoichiometric composition (Bi,Pb) one would expect $q(\mathrm{Mn}) = 3.5|e|$.

Bond Distances and Coordination Polyhedra

Relevant interatomic distances are reported in Table 5 for the *Amaa* and *Fmmm* refinements, and compared to the corresponding ones from the average structure of Cu-2212 (8). Manganese shows a distorted octahedral coordination, with O5 providing the sixth corner shared between two octahedra of adjacent Mn layers; this contrasts with the cuprate structure, where copper has a fivefold pyramidal surrounding. The Mn–O3 bond, approximately parallel to z at about 180° from Mn–O5, is the longest one and indicates a Jahn–Teller distortion on a single side of the octahedron. However, the average Mn–O distance (1.98 Å) is closer to the ideal value for Mn^{4+} (1.94 Å) than to that of Mn^{3+} (2.05 Å), on the basis of the sum of the corresponding ionic radii with that of oxygen (15). In the case of the Mn-2201 phase ($BiPbSr_2MnO_6$), the Mn–O distances were 1.893×4 (intralayer) and 2.328×2 Å (parallel to z), with $\langle \mathrm{Mn–O} \rangle = 2.038$ Å, which agrees perfectly with what is expected for Mn^{3+} with a full bilateral Jahn–Teller distortion of the coordination octahedron (5). By computing the

TABLE 5
Individual and Average Interatomic Distances (Å) Within Metal–Oxygen Coordination Polyhedra for *Amaa* and *Fmmm* Spage Groups

	Mn-2212 (*Amaa*)	Mn-2212 (*Fmmm*)	Cu-2212 (8) (*Amaa*)
Mn–O1	1.895(16) × 2	1.903(3) × 2	1.914 × 2
Mn–O2	1.943(16) × 2	1.936(5) × 2	1.913 × 2
Mn–O3	2.228(15)	2.217(14)	2.484
Mn–O5	1.952(7)	1.951(6)	—
Average (C.N. = 6)	1.976	1.974	2.028
(Bi,Pb)–O3	2.097(14)	2.107(14)	1.991
(Bi,Pb)–O4 1	2.019(22)	1.998(20)	2.092
(Bi,Pb)–O4 2	2.387(26)	2.387(24)	2.724
(Bi,Pb)–O4 3	3.137(22)	3.143(21)	2.766
(Bi,Pb)–O4 5	3.142(20)	3.147(20)	3.411
(Bi,Pb)–O4 4	3.412(19)	3.434(17)	3.340
Average (C.N. = 5)	2.406, 2.556, 2.706		2.393
(Sr1,Ca1)–O1	2.734(21) × 2	2.735(18) × 2	2.617 × 2
(Sr1,Ca1)–O2	2.313(18) × 2	2.329(13) × 2	2.596 × 2
(Sr1,Ca1)–O3	2.707(4) × 2	2.703(2) × 2	2.811 × 2
(Sr1,Ca1)–O3	2.77(9)	2.722(2) × 2	2.656
(Sr1,Ca1)–O3	2.68(9)		2.966
(Sr1,Ca1)–O4	2.628(21)	2.637(20)	2.647
Average (C.N. = 9)	2.621	2.624	2.702
(Sr2,Ca2)–O1	2.582(16) × 4	2.573(16) × 4	2.491 × 4
(Sr2,Ca2)–O2	3.030(16) × 4	3.025(16) × 4	2.497 × 4
(Sr2,Ca2)–O5	2.6848(1) × 2	2.6848(1) × 2	—
(Sr2,Ca2)–O5	2.6657(1) × 2	2.6657(1) × 2	—
Average (C.N. = 8)	2.629	2.624	2.494
Average (C.N. = 12)	2.762	2.758	

Note. Results are compared to those on BSCCO-2212 from Ref. (8).

bond-valence sum (16) on Mn in the present compound, one obtains 3.5 $|e|$, which is slightly lower than the value 3.8 $|e|$ derived above from the site occupancy refinement and charge balance constraints, but it confirms a substantial degree of oxidation of Mn^{3+}.

As for the two-layer rock salt block, the main feature is the positional disorder of O4 across the (100) (*Amaa*) and (010) (*Fmmm*) mirror planes. This O4 split-atom configuration resembles that previously observed for the Mn-2201 phase (5), as far as the (100) plane disorder is concerned. The (Bi,Pb)–O4 contacts denoted by 1, 2, 3, 4 (cf. Table 5, and Fig. 2) lie in the layer, while the other two are approximately perpendicular to it. In space group *Amaa* the contacts 1 and 4 are fully ordered, owing to the absence of the (010) *m* plane; on the other hand, bonds 2 and 3 can be associated in pairs 2.39–2.39 (2–2), 2.39–3.14 (2–3), or 3.14–3.14 (3–3), according to the locally ordered configuration taken by O4. This pattern is likely to be correlated to the (Bi,Pb) site being (a) occupied by Bi^{3+}, (b) occupied by Pb^{2+}, or (c) vacant. In the first case, we expect O4 to be located most probably so as to give two short bonds of 2.39 Å (the ideal Bi–O bond length is 2.43 Å), while in case (b) a short and a long bond should be likely (ideal Pb–O = 2.59 Å), and in case (c) both long distances (3.41 Å) should be expected. The corresponding three average values of (Bi,Pb)–O distances are given in Table 5; the longest contact of 3.412 Å is excluded from the coordination surrounding, so that the C.N. is 5, corresponding to the well-known stereochemical effect of the $6s^2$ lone pair of Bi and Pb. In the fully disordered *Fmmm* space group, the pattern of locally ordered configurations would be much more complicated, because the 1 and 4 contacts are also involved.

A comparison with the Bi–O layer configuration in the cuprate structure shows that, in the latter case: (i) adjacent Bi–O layers are more spaced (3.41 against 3.14 Å for the interlayer contact 5), while each layer approaches the neighboring Sr–O3 plane (1.99 against 2.10 Å for the Bi–O3 bond); (ii) the pattern of Bi–O bonds within the layer is much less distorted (cf. bond distances 2 and 3). This is consistent with an easier transfer of charge carriers within the Bi–O layer and from that layer to the Sr–O and Cu–O planes, with respect to Mn-2212, where the two-layer rock salt block is more isolated from the rest of the structure.

Let us consider, eventually, the coordination polyhedra around (Ca1,Sr1) and (Sr2,Ca2) sites: in the first case the average metal–oxygen distance for C.N. = 9 (2.62 Å) has to be compared with 2.71 and 2.58 Å for Sr–O and Ca–O, respectively, from sums of ionic radii (15). In the second case an average bond length of 2.64 Å is observed, assuming C.N. = 8, against ideal values of 2.66 (Sr–O) and 2.52 (Ca–O) Å. Simple linear interpolations would thus give 70% Ca in site 1 and 85% Sr in site 2, in general agreement with the refined occupancy factors of the two sites. By considering the corresponding average of metal–oxygen bond lengths of the Cu-2212 structure, it appears clearly that Sr and Ca are fully ordered in site 1 and site 2, respectively. Such different crystal-chemical behavior of the Mn and Cu phases is probably related to the need of accommodating in the Mn-2212 compound the additional O5 oxygen within the (Sr2,Ca2) layer for charge balance reasons. This leads to an expansion of the spacing between adjacent Mn–O layers, which in turn favors the presence of Sr in place of Ca in site 2. Enrichment of Ca in site 1 follows from chemical composition.

ACKNOWLEDGMENTS

The experiment at Brookhaven National Laboratory was supported by contract DE-AC02-76CH00016 with US DOE by its Division of Chemical Science Office of Basic Energy Sciences. The National Research Council (C.N.R.), Italy, is gratefully acknowledged for financial support and for the use of the A.R.L. microprobe at the Centro di Studio per la Geodinamica Alpina e Quaternaria (Milano, Italy). We thank Luca Toia and Francesco Moneta for their help with the synthesis of the compound studied in this work.

REFERENCES

1. C. C. Torardi, M. A. Subramanian, J. C. Calabrese, J. Gopalakrishnan, E. M. McCarron, K. J. Morissey, T. R. Askew, R. B. Flippen, U. Chowdry, and A. W. Sleight, *Phys. Rev. B* **38,** 225 (1988).
2. J. M. Tarascon, Y. LePage, W. R. McKinnon, R. Ramesh, M. Eibschutz, E. Tselepis, E. Wang, and G. W. Hull, *Physica C* **167,** 20 (1990).
3. M. Catti, G. Dalba, P. Fornasini, and M. Mölgg, *J. Solid State Chem.* **112,** 392 (1994).
4. W. R. McKinnon, E. Tselepis, J. M. Tarascon, P. F. Miceli, K. Remschnig, and G. W. Hull, *Phys. Rev. B* **43,** 5468 (1991).
5. D. Levy, W. T. Fu, D. J. W. Ijdo, and M. Catti, *Solid State Commun.* **92,** 659 (1994).
6. C. B. Azzoni, M. Catti, A. Paleari, and C. Pogliani, *J. Phys. Condens. Matter* **9,** 3931 (1997).
7. M. Hervieu, C. Michel, D. Pelloquin, A. Maignan, and B. Raveau, *J. Solid State Chem.* **132,** 420 (1997).
8. Y. Gao, P. Coppens, D. E. Cox, and A. R. Moodenbaugh, *Acta Cystallogr. A* **49,** 141 (1993).
9. A. C. Larson and R. B. Von Dreele. GSAS: Generalized Structure Analysis System manual. Los Alamos National Laboratory Report. LAUR 86–748, 1994.
10. C. J. Howard, *J. Appl. Crystallogr.* **15,** 615 (1982).
11. P. Thompson, D. E. Cox, and J. B. Hastings, *J. Appl. Crystallogr.* **20,** 79 (1987).
12. K. Kuroda, N. Ishizawa, N. Mizutani, and M. Kato, *J. Solid State Chem.* **38,** 297 (1981).
13. A. W. Hewat, *Acta Crystallogr. A* **35,** 248 (1979).
14. Y. Lepage, W. R. McKinnon, J. M. Tarascon, and P. Barboux, *Phys. Rev. B* **40,** 6810 (1989).
15. R. D. Shannon, *Acta Crystallogr. A* **32,** 751 (1976).
16. I. D. Brown and D. Altermatt, *Acta Crystallogr. B* **41,** 244 (1985).